Mon. Not. R. Astron. Soc. **263,** 545–559 (1993)

Collimation effects of the Kerr field

J. Bičák,[1,2] O. Semerák[1] and P. Hadrava[3]

[1] *Department of Theoretical Physics, Faculty of Mathematics and Physics, Charles University, V Holešovičkách 2, 180 00 Praha 8, Czech Republic*
[2] *Institute of Astronomy, University of Cambridge, Madingley Road, Cambridge CB3 0HA*
[3] *Astronomical Institute, Academy of Sciences, 251 65 Ondřejov, Czech Republic*

Accepted 1993 January 3. Received 1992 September 30

ABSTRACT

The latitudinal motion of free test particles outwards from central regions in the Kerr geometry is investigated analytically and by the numerical integration of geodesic equations. Compared to particles with parabolic energies, particles with hyperbolic energies escape closer to the rotation axis, while slower particles tend to fall towards the equatorial plane. The effect is not large in the case of Kerr black holes, but it is significant for Kerr naked singularities. In the region even closer to the centre, the repulsive character of the field near the rotation axis and near the disc spanning the Kerr ring singularity gives particles outward accelerations and collimates them along the rotation axis. Here, low-energy particles are more collimated than are those with high energies. These results might be relevant in the context of the formation and pre-collimation of cosmic jets.

Key words: black hole physics – relativity – galaxies: jets.

1 INTRODUCTION

Although there is no direct observational evidence available, it is generally believed that cosmic jets emerging from quasars and active galactic nuclei are initiated on scales of the order of the size of a central engine. Whatever the mechanism of their production, the jets are assumed to propagate along the direction indicated by the central source, in other words, as is generally believed, along the rotation axis of a compact relativistic object, most probably a rapidly rotating Kerr black hole (Begelman, Blandford & Rees 1984). As experts in the field emphasize, 'the major unsolved problem is to understand how and where jets are collimated' (Blandford 1987).

In this work, we do not attempt to treat this problem in all its complexity. However, we wish in this context to examine a simple question which, perhaps surprisingly, does not yet appear to have been properly addressed: could not the gravitational field of the central source, i.e. – as is generally supposed – that of the Kerr geometry itself, possibly help in the (pre-)collimation of particles, ejected from the vicinity of the source by some process, along the rotation axis? We discuss this question by studying trajectories, in particular the latitudinal and radial motion, of free test particles moving outwards in the Kerr geometry from given positions and under given initial conditions. We thus deal with idealized situations in which other complex processes are not considered, and only the geometry produced by a rotating compact relativistic source is taken into account.

A great deal of effort has been devoted to studies of the particle orbits in the Kerr geometry (for reviews, see, for example, Sharp 1979; Chandrasekhar 1983; Dymnikova 1986; Bičák, Stuchlík & Balek 1989a,b). Although most authors consider only qualitative features of the motion by means of effective potentials, some papers also contain specific trajectories constructed numerically. Leaving aside equatorial geodesics, we may mention numerical investigations of the dragging effects (Johnston & Ruffini 1974; Goldstein 1974; Stoghianidis & Tsoubelis 1987), of the motion of particles through the ergosphere (Contopoulos 1984) and of causality-violating null trajectories (de Felice & Calvani 1979). Some numerically constructed trajectories are also given by Chandrasekhar (1983), including those around the Kerr naked singularity; in his words, 'considerable interest attaches to knowing the sort of things space-times with naked singularities are and whether there are any essential differences in the manifestations of space-times with singularities concealed behind event horizons'. In the context of the present paper, we should in particular mention the work of Floyd & Sheppee (1972), who studied how the region around the Kerr naked singularity is seen by an observer outside the equatorial plane: they constructed the photon trajectories and plotted them in Kerr–Schild coordinates. Finally, the work of Lake, Hood & Stone (1984) was devoted to the numerical study of the latitudinal and radial motion of the particles in the Kerr metric. However, no collimation effects were discovered in this last work, and the repulsive region around the Kerr ring

singularity, which plays a crucial role in the motion, escaped notice. In Appendix B, we discuss the conclusions of the paper by Lake et al. (1984) in the light of our results.

In our work we do find collimation effects: particles with hyperbolic energies tend to move closer to the rotation axis as compared with slower particles, the effect being fairly strong in the case of naked Kerr singularities. Moreover, the repulsive region near the disc spanning the Kerr ring singularity can collimate (and accelerate) particles considerably.

As is well known, according to the cosmic censorship hypothesis and the uniqueness theorems for black holes, the outcome of the gravitational collapse of a sufficiently massive rotating star is a rotating Kerr black hole, rather than a Kerr naked singularity. Nevertheless, although cosmic censorship is a very plausible hypothesis, it remains one of the central unresolved issues in classical relativity; in recent years there appears to have grown up a body of evidence against it. Naked singularities arise in various treatments of spherically symmetric collapse (for the most recent one, see Lake & Zannias 1990). In connection with the collapse of rotating stars, it was primarily de Felice and his co-workers (de Felice & Yu 1982; Miller & de Felice 1985) who argued that, although mass shedding and gravitational radiation will reduce the star's angular momentum during collapse, it will not in general be reduced to the value that corresponds to a Kerr black hole. De Felice (1975) also investigated some physical properties of the Kerr naked singularity, in particular its repulsive effects (see also more recent work by de Felice & Bradley 1988). It appears to follow, from the extensive 2D numerical work of Nakamura, Oohara & Kojima (1987), that a rotating, collapsing supermassive star will not always dissipate enough angular momentum to form a black hole, but that instead, for rather rapidly rotating models, a Kerr-like naked singularity might be expected to develop. Recently, Charlton & Clarke (1990) analysed a possible scenario for the evolution of a collapsing rotating star from an initially regular state to a final state described by the naked Kerr geometry with a ring singularity. Furthermore, Shapiro & Teukolsky (1992, and references therein) explored numerically the collapse of collisionless gas spheroids, and found 'strong candidates for the formation of naked singularities in general relativity'.

In the present paper, after writing down in Section 2 basic relations for the test particle motion in the Kerr metric, we define and analyse possible collimation effects analytically (Section 3). The Carter equations are used directly, and some qualitative features of the motion are also deduced from the effective potentials for the latitudinal motion. In the last part of Section 3, Kerr–Schild coordinates are introduced in order to describe properly the inner regions of the Kerr geometry. As the results of Section 3 show, however, only direct numerical integration of the geodesic equations yields the real trajectory and can inform us about collimation effects. Typical pictures of trajectories obtained numerically are presented and discussed in Section 4. Concluding remarks then follow in Section 5. In Appendix A, constants of motion are expressed in terms of quantities directly measurable in various local frames tied to observers orbiting around the centre. In addition, as already mentioned above, the numerical work of Lake et al. (1984) that is relevant for the problem of collimation is discussed in Appendix B.

Some of the results contained in this paper were reported at the Sixth Marcel Grossmann Meeting on General Relativity in Kyoto in 1991 (Bičák, Semerák & Hadrava 1992).

2 GEODESIC MOTION IN THE KERR METRIC

In studying the test particle motion in the Kerr metric, it is advantageous to use the Boyer–Lindquist (BL) coordinate system $(x^\mu)=(x^0, x^1, x^2, x^3)=(t, r, \theta, \varphi)$, because in these coordinates the geodesic equations are separable. The BL coordinates also follow naturally from the symmetries of the Kerr space-time. The scalars t and φ can be fixed uniquely (up to additive constants) as parameters varying along the integral curves of (unique) stationary and axial Killing vector fields $\boldsymbol{\xi}$ and $\boldsymbol{\zeta}$, and the scalars r and θ can be fixed (up to constant factors) as parameters related as closely as possible to the – geometrically preferred – principal null congruences and their projections on to the two-dimensional space-like submanifolds orthogonal to both $\boldsymbol{\xi}$ and $\boldsymbol{\zeta}$ (see Stewart & Walker 1973 for details). BL coordinates represent the natural generalization of Schwarzschild coordinates in Schwarzschild space-time.

In BL coordinates and in geometrized units $c=G=1$, the Kerr metric characterized by the mass M and the angular momentum J takes the form

$$\mathrm{d}s^2=-\frac{\Delta\Sigma}{\mathscr{A}}\mathrm{d}t^2+\frac{\mathscr{A}}{\Sigma}\sin^2\theta(\mathrm{d}\varphi-\omega\,\mathrm{d}t)^2+\frac{\Sigma}{\Delta}\mathrm{d}r^2+\Sigma\,\mathrm{d}\theta^2, \quad (1)$$

where

$$\Delta=r^2-2Mr+a^2, \qquad \Sigma=r^2+a^2\cos^2\theta,$$

$$\mathscr{A}=(r^2+a^2)^2-\Delta a^2\sin^2\theta, \quad (2)$$

$$\omega=2Mar/\mathscr{A}=-g_{t\varphi}/g_{\varphi\varphi}, \quad (3)$$

and $a=J/M$; $0\le a\le M$ corresponds to a black hole, $a>M$ to a naked singularity.

Carter's equations, the first integrals of the equations of motion of a free test particle, read

$$\Sigma\dot{t}=(r^2+a^2)\frac{P}{\Delta}-aT\sin\theta=\frac{\mathscr{A}}{\Delta}(E-\omega\Phi), \quad (4)$$

$$\Sigma^2\dot{r}^2=R(r)=P^2-\Delta(m^2r^2+K), \quad (5)$$

$$\Sigma^2\dot{\theta}^2=\Theta(\theta)=K-(ma\cos\theta)^2-T^2, \quad (6)$$

$$\Sigma\dot{\varphi}=a\frac{P}{\Delta}-\frac{T}{\sin\theta}=\frac{1}{\Delta}\left(\mathscr{A}\omega E+\frac{\Sigma-2Mr}{\sin^2\theta}\Phi\right) \quad (7)$$

(Carter 1968). Here, the particle's rest mass, m, its energy at infinity, E, the azimuthal component of its angular momentum at infinity, Φ, and the modified Carter 'fourth constant' K (in the Schwarzschild limit this is the square of the total angular momentum at infinity) are constants of motion, functions P and T are given by

$$P=(r^2+a^2)E-a\Phi, \qquad T=aE\sin\theta-\Phi/\sin\theta,$$

and the dot denotes differentiation with respect to the affine parameter λ, normalized so that the 4-momentum is $p^\mu=\dot{x}^\mu$. Appendix A gives the parametrization of constants of motion

in terms of quantities measured with respect to different frames carried by local observers.

3 THE COLLIMATION OF PARTICLES IN THE KERR GEOMETRY: ANALYTIC CONSIDERATIONS

Let a particle reach an 'initial' position $(r_{\rm in}, \theta_{\rm in}, \varphi_{\rm in})$ outside the event horizon of a Kerr black hole, or outside a Kerr naked singularity. Let us assume that a mechanism exists which gives the particle an initial velocity $\hat{v}_{\rm in}$ in the direction $\hat{\alpha}_{\rm in}$, $\hat{\beta}_{\rm in}$, as measured in a local frame at the initial position – see Fig. 1. In the following, standard 'locally non-rotating frames' (LNRFs) (Bardeen, Press & Teukolsky 1972), tied to the zero-angular-momentum observers, are used most frequently, but other frames, such as the Carter frame (Znajek 1977; Carter 1987) or the frame connected with freely orbiting particles, will also be employed. Quantities measured in a general frame are denoted by a hat and by a capital F under the quantity (in particular, in the LNRF we use just hats), and other symbols are used in the cases of other frames (see Appendix A for details).

Our main concern is to see how the latitude θ of the particle will evolve as a function of the radial coordinate r, which characterizes the distance from the central rotating object. What is the dependence of the shape of the orbit $r(\theta)$ and, in particular, of a possible collimation along the rotation axis on $r_{\rm in}$, $\theta_{\rm in}$, $\hat{v}_{\rm in}$, $\hat{\alpha}_{\rm in}$ and $\hat{\beta}_{\rm in}$ or, alternatively, on $r_{\rm in}$, $\theta_{\rm in}$, E, Φ and K?

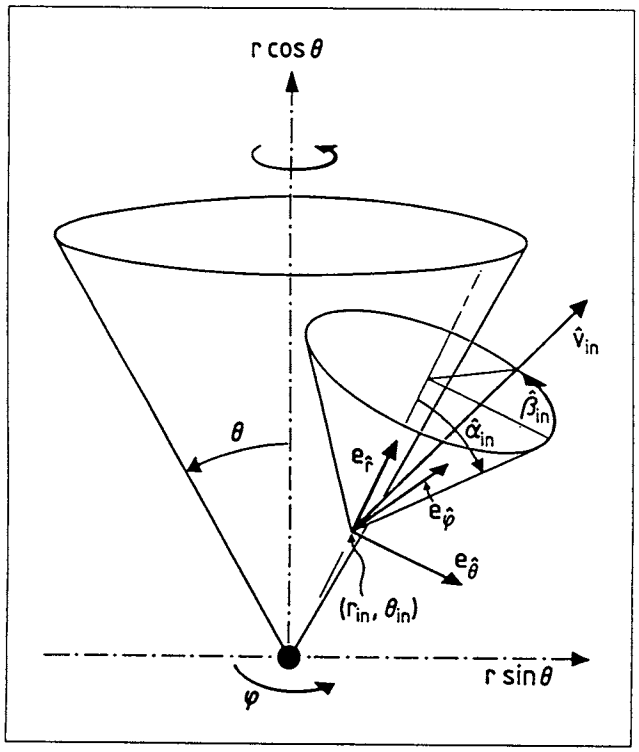

Figure 1. The particle is ejected from a point $(r_{\rm in}, \theta_{\rm in})$, the azimuthal coordinate $\varphi_{\rm in}$ being suppressed because of axisymmetry. The particle's initial velocity is represented by its magnitude $\hat{v}_{\rm in}$, by the local latitude $\hat{\alpha}_{\rm in}$, and by the local azimuth $\hat{\beta}_{\rm in}$, as measured with respect to the orthonormal basis $\{e_{\hat{r}}, e_{\hat{\theta}}, e_{\hat{\varphi}}\}$ of the locally non-rotating frame (LNRF) at $(r_{\rm in}, \theta_{\rm in})$.

Clearly, the shapes of the orbits depend on the coordinates used to illustrate them. BL coordinates represent the appropriate grid for discussion of the latitudinal behaviour of the orbits, for several reasons: (i) they are geometrically preferred, as mentioned in Section 2; (ii) the surfaces θ = constant represent a natural generalization of surfaces θ = constant in the Schwarzschild space-time: particles with zero angular momentum, $\Phi = 0$, fall from rest at infinity towards the centre along θ = constant; they fall radially with respect to LNRFs but, of course, are dragged around with respect to the static observers at φ = constant (see Bičák & Stuchlík 1976a for more details); and (iii) the PNC photons, the photons moving along the principal null congruences in Kerr space-time, which are thus best 'moulded' into the Kerr geometry, move along θ = constant in BL coordinates. Because of all of these facts, a particle ejected radially with respect to the LNRF ($\hat{\alpha}_{\rm in} = 0$) at $r_{\rm in}$, $\theta_{\rm in}$, and which then moves towards the rotation axis (i.e. towards $\sin\theta < \sin\theta_{\rm in}$), can be considered as 'being collimated'. In the non-rotating (Schwarzschild) case, such a particle would continue to move along θ = constant.

However, BL coordinates do not properly represent the Kerr disc $r = 0$, $\theta \neq \pi/2$ which is spanning the Kerr singularity $r = 0$, $\theta = \pi/2$; the whole disc is mapped into the origin in the plots with $r\sin\theta$, $r\cos\theta$ as axes. In order to describe the neighbourhood of the Kerr disc properly, we shall employ Kerr–Schild coordinates; these will be described in the last part of this section (3.4).

Before presenting numerical results, we shall study some effects analytically. The general features of the motion of test particles are usually studied by means of effective potentials – we shall discuss them in Section 3.3. First, we shall try to find out whether some collimation effects can be inferred directly from the equations of motion, or from their first integrals.

3.1 Close to the starting point of a particle's trajectory

Expressing K in terms of the initial values of quantities measured in a local frame by equations (A4) and (A9), we find that the equation for latitudinal motion (6) has the form

$$\Sigma^2\dot{\theta}^2 = a^2(m^2 - E^2)(\sin^2\theta - \sin^2\theta_{\rm in}) + \Phi^2(\sin^{-2}\theta_{\rm in} - \sin^{-2}\theta) + \Sigma_{\rm in}(\hat{L}_{\rm in}\, v^{\hat{\theta}}_{\rm in})^2. \quad (8)$$

It is immediately seen that, for the particles with small initial angular components of velocity (i.e. small Φ and $v^{\hat{\theta}}_{\rm in}$), the first term on the right-hand side of equation (8) is dominant. Since the right-hand side of equation (8) must be positive, such particles will, at least initially, move towards the axis of symmetry, $\sin^2\theta < \sin^2\theta_{\rm in}$, if $m^2 - E^2 < 0$, i.e. their energies are hyperbolic. This condition is always satisfied by photons ($m = 0$), and even better by tachyons, which have imaginary m, τ and $\sqrt{1 - \hat{v}^2}$, and thus 'move' along space-like geodesics. This is not to say that we attribute a physical meaning to the tachyons as real particles, but it is of interest to see how space-like geodesics behave in the Kerr geometry, and that is why we also touch on tachyons in our discussion and include them in some of our numerical results. On the other hand, particles with elliptic energies ($m^2 > E^2$), or those with large Φ, $v^{\hat{\theta}}_{\rm in}$, will start to move away from the axis of symmetry.

One can obtain more insight into the role of individual terms from the 'latitudinal acceleration':

$$\frac{\mathrm{d}}{\mathrm{d}\lambda}(r\dot{\theta})=\frac{a^2 r}{2\Sigma^2}(m^2-E^2)\sin 2\theta+\frac{r\cos\theta}{\Sigma^2\sin^3\theta}\Phi^2$$

$$+\left(1-\frac{2r^2}{\Sigma}\right)\dot{r}\dot{\theta}+\frac{a^2 r}{\Sigma}\dot{\theta}^2\sin 2\theta. \qquad (9)$$

The second and third terms are 'inherited', with small modifications, from the Schwarzschild case or, rather, from the Newtonian treatment of the motion in a spherically symmetric force field. These terms become less important as the rotation parameter a increases. The first and last terms arise only if $a\neq 0$, and they are thus important for collimation. In particular, the first term leads to the collimation of particles with hyperbolic energies.

As indicated above, whenever the azimuthal angular momentum Φ is large, we can, on already Newtonian grounds, hardly expect that ejected particles will be noticeably collimated towards the axis. Hence, in order to see most clearly the effect of the Kerr geometry, we shall now consider the particles that are ejected purely radially outwards as measured in the LNRFs. Such particles have $v^{\hat{\theta}}_{\mathrm{in}}=v^{\hat{\varphi}}_{\mathrm{in}}=0$ and thus $\Phi=0$, $K=a^2[(E^2-m^2)\sin^2\theta_{\mathrm{in}}+m^2]$, as follows from (A10) and (A4). Equations (8) and (9) then simplify to

$$\Sigma^2\dot{\theta}^2=a^2(m^2-E^2)(\sin^2\theta-\sin^2\theta_{\mathrm{in}}), \qquad (10)$$

$$\frac{\mathrm{d}}{\mathrm{d}\lambda}(r\dot{\theta})=\frac{a^2 r}{2\Sigma^2}(m^2-E^2)\sin 2\theta+\left(1-\frac{2r^2}{\Sigma}\right)\dot{r}\dot{\theta}$$

$$+\frac{a^2 r}{\Sigma}\dot{\theta}^2\sin 2\theta. \qquad (11)$$

According to (10), an accessible region of latitudes θ for particles with hyperbolic energies is $\langle 0,\ \theta_{\mathrm{in}}\rangle$ (and $\langle \pi,\ \pi-\theta_{\mathrm{in}}\rangle$ as a result of the symmetry with respect to the equatorial plane), whereas particles with elliptic energies are confined to the latitudes $\langle \theta_{\mathrm{in}},\ \pi-\theta_{\mathrm{in}}\rangle$. Particles with parabolic energies continue to move along $\theta=\theta_{\mathrm{in}}$, as would all particles in the Schwarzschild geometry regardless of their energy. At the starting points of the trajectories of those particles ejected radially outwards in LNRFs, $\dot{\theta}_{\mathrm{in}}=0$, and the latitudinal acceleration (11) is simply given by

$$\left[\frac{\mathrm{d}}{\mathrm{d}\lambda}(r\dot{\theta})\right]_{\mathrm{in}}=r_{\mathrm{in}}\ddot{\theta}_{\mathrm{in}}=\frac{a^2 r_{\mathrm{in}}}{2\Sigma_{\mathrm{in}}^2}(m^2-E^2)\sin 2\theta_{\mathrm{in}}. \qquad (12)$$

We see again that particles with hyperbolic energies are deflected towards the axis of symmetry – the larger E is, the greater the collimation to be expected.

It is instructive to see how latitudes change if the particles are ejected radially with respect to frames tied to observers with some angular momentum (and thus orbiting in the φ-direction with respect to LNRFs). The Carter frame (CF) is one of the privileged frames of this type. The PNC photons move radially in the CFs, and we would thus intuitively expect that particles with non-zero rest mass ejected radially outwards as measured in the CFs would start to move away from the rotation axis, whereas tachyons would still be collimated towards the axis. Indeed, this is so. A particle ejected radially in the CF will have $v^{\hat{\theta}}_{\mathrm{in}}=v^{\hat{\varphi}}_{\mathrm{in}}=0$ and thus $\Phi=aE\sin^2\theta_{\mathrm{in}}$ and $K=(ma\cos\theta_{\mathrm{in}})^2$, as follow from (A12), (A13) and (A4). Equations (8) and (9) then yield

$$\Sigma^2\dot{\theta}^2=a^2(m^2-E^2+E^2\sin^2\theta_{\mathrm{in}}/\sin^2\theta)(\sin^2\theta-\sin^2\theta_{\mathrm{in}}), \qquad (13)$$

$$\frac{\mathrm{d}}{\mathrm{d}\lambda}(r\dot{\theta})=\frac{a^2 r\cos\theta}{\Sigma^2\sin^3\theta}[(m^2-E^2)\sin^4\theta+E^2\sin^4\theta_{\mathrm{in}}]$$

$$+\left(1-\frac{2r^2}{\Sigma}\right)\dot{r}\dot{\theta}+\frac{a^2 r}{\Sigma}\dot{\theta}^2\sin 2\theta. \qquad (14)$$

According to (13), an accessible region of latitudes for tachyons ($m^2<0$) is $\langle\theta_0,\ \theta_{\mathrm{in}}\rangle$ (and $\langle\theta_{\mathrm{in}},\ \pi-\theta_0\rangle$), where $\theta_0=\arcsin(E\sin\theta_{\mathrm{in}}/\sqrt{E^2-m^2})<\theta_{\mathrm{in}}$, whereas, for particles with $1\geq\tilde{v}^2_{\mathrm{in}}\geq 1-(\Delta_{\mathrm{in}}/\Sigma_{\mathrm{in}})\cos^2\theta_{\mathrm{in}}$ (which implies that $E\geq m/|\cos\theta_{\mathrm{in}}|\geq m$), the latitudes are confined to $\langle\theta_{\mathrm{in}},\ \theta_0\rangle$ (and $\langle\pi-\theta_0,\ \theta_{\mathrm{in}}\rangle$) and, for still less energetic particles, $\theta\in\langle\theta_{\mathrm{in}},\ \pi-\theta_{\mathrm{in}}\rangle$. In addition, the latitudinal acceleration (14) at the starting point of the trajectory reduces to

$$\left[\frac{\mathrm{d}}{\mathrm{d}\lambda}(r\dot{\theta})\right]_{\mathrm{in}}=r_{\mathrm{in}}\ddot{\theta}_{\mathrm{in}}=\frac{a^2 r_{\mathrm{in}}}{2\Sigma_{\mathrm{in}}^2}m^2\sin 2\theta_{\mathrm{in}}, \qquad (15)$$

which shows that tachyons ($m^2<0$) are bent towards the rotation axis, while massive particles ($m^2>0$) start to move towards the equatorial plane; and, as expected, the photons ($m^2=0$) – which are just the PNC photons – escape along constant $\theta=\theta_{\mathrm{in}}$.

The same conclusions may be drawn directly from the shape of the particle's trajectory in the (ρ, z)-plane, where $\rho=r\sin\theta$, $z=r\cos\theta$. Its first curvature, $C=(\dot{\rho}\ddot{z}-\ddot{\rho}\dot{z})/(\dot{\rho}^2+\dot{z}^2)^{3/2}$, at the starting point of a particle ejected with $\dot{\theta}_{\mathrm{in}}=0$, is just equal to $C_{\mathrm{in}}=-r_{\mathrm{in}}\ddot{\theta}_{\mathrm{in}}/\dot{r}^2_{\mathrm{in}}$. In the case of a particle ejected radially in the LNRF, this becomes

$$C_{\mathrm{in}}=a^2 r_{\mathrm{in}}(E^2-m^2)\sin 2\theta_{\mathrm{in}}/(2\Delta_{\mathrm{in}}\Sigma_{\mathrm{in}}\hat{E}^2_{\mathrm{in}}\hat{v}^2_{\mathrm{in}}),$$

while, for a particle ejected radially in the CF, one finds

$$C_{\mathrm{in}}=-a^2 r_{\mathrm{in}}m^2\sin 2\theta_{\mathrm{in}}/(2\Delta_{\mathrm{in}}\Sigma_{\mathrm{in}}\tilde{E}^2_{\mathrm{in}}\tilde{v}^2_{\mathrm{in}}).$$

Particles with parabolic energy represent the 'dividing' (uncollimated) line in the first case, whereas (PNC) photons do so in the second case.

3.2 Close to the 'end-point' of an unbound trajectory

In order to understand possible collimation effects in the Kerr field, it would be useful to find some global characteristics of the particle motion that are directly connected with the latitudinal angle, θ_∞, with which a particle (with $E\geq m$) arrives at infinity. Conserved quantities E, Φ and K suggest themselves in this respect. Thus the question arises as to whether θ_∞ cannot be determined in terms of these constants of motion. In Appendix A, the constants of motion are expressed in terms of quantities measured locally in frames tied to observers orbiting along the φ-lines. We shall now use the LNRFs in our discussion, but any set of frames orbiting along $(r,\theta)=$ constant, which go over into the frames of static observers at $r\to\infty$, could be considered. At first sight, it might appear that the four relations (A3), (A4), (A10) and (A11), when considered in the limit $r\to\infty$, might enable us to express θ_∞ (and, possibly, also $\hat{\alpha}_\infty$ and $\hat{\beta}_\infty$) in terms of

E, Φ and K, just as the asymptotic value $\hat{v}_\infty$ can be expressed, by using (A11), in terms of just E as

$$\hat{v}_\infty = (1 - m^2/E^2)^{1/2}. \tag{16}$$

In this manner, θ_∞ could be determined by means of the particle's initial position and velocity.

Let us introduce

$$d = r \sin \hat{\alpha}, \tag{17}$$

which determines the impact parameter

$$d_\infty = \lim_{r \to \infty} d \tag{18}$$

for trajectories reaching infinity. We easily see that, as $r \to \infty$, (A10), (A11) and (A4) imply that

$$\Phi = \hat{E}_\infty \hat{v}_\infty d_\infty \sin \hat{\beta}_\infty \sin \theta_\infty, \tag{19}$$

$$E = \hat{E}_\infty = m/\sqrt{1 - \hat{v}_\infty^2}, \tag{20}$$

$$K = (ma \cos \theta_\infty)^2 + (aE \sin \theta_\infty - \Phi/\sin \theta_\infty)^2 - (\hat{E}_\infty \hat{v}_\infty d_\infty \cos \hat{\beta}_\infty)^2. \tag{21}$$

By expanding functions of r entering (A3) for $r \to \infty$, we first obtain

$$K = E^2(r^2 + 2Mr + 4M^2 + a^2) - 2aE\Phi - (m^2 + \hat{E}^2\hat{v}^2)r^2 + \hat{E}^2\hat{v}^2(d^2 - a^2 \cos^2 \theta) + O(1/r). \tag{22}$$

Using (A11) to find an asymptotic relation between E and $\hat{E}$,

$$\hat{E}^2 r^2 = E^2(r^2 + 2Mr + 4M^2) + O(1/r),$$

and substituting this back into (22), we can make sure that all terms in (22) that depend on positive powers of r cancel out. At infinity, we therefore obtain

$$K = a^2E^2 - 2aE\Phi + E^2\hat{v}_\infty^2(d_\infty^2 - a^2 \cos^2 \theta_\infty). \tag{23}$$

Expressing $\hat{v}_\infty$ in (19), (21) and (23) in terms of E by use of (16), we arrive at the following three relations:

$$\Phi = (E^2 - m^2)^{1/2} d_\infty \sin \hat{\beta}_\infty \sin \theta_\infty, \tag{24}$$

$$K = (ma \cos \theta_\infty)^2 + (aE \sin \theta_\infty - \Phi/\sin \theta_\infty)^2 - (E^2 - m^2) d_\infty^2 \cos^2 \hat{\beta}_\infty, \tag{25}$$

$$K = a^2E^2 - 2aE\Phi + (E^2 - m^2)(d_\infty^2 - a^2 \cos^2 \theta_\infty). \tag{26}$$

Together with (16), the last three results do not, however, determine all asymptotic quantities $\hat{v}_\infty$, θ_∞, $\hat{\beta}_\infty$, d_∞ in terms of constants of motion, because (24), (25) and (26) are not independent. Equations (26) and (24) yield[1]

$$\cos^2 \theta_\infty = \frac{1}{a^2}\left(d_\infty^2 + \frac{a^2E^2 - 2aE\Phi - K}{E^2 - m^2}\right). \tag{27}$$

The asymptotic latitude, θ_∞, is just expressed in terms of the constants of motion and the impact parameter d_∞, which remains unknown.

[1]The formula (27) is in agreement with the equatorial and axial components of the impact parameter as given by Bardeen (1973), Dymnikova (1986) and Yakovlev (1975) (denoted by α and β, $\rho_\perp$ and $\rho_\parallel$, and ρ_1 and ρ_2, respectively). The relations are $-\alpha = \rho_\perp = \rho_1 = d_\infty \sin \hat{\beta}_\infty$ and $\beta = \rho_\parallel = \rho_2 = d_\infty \cos \hat{\beta}_\infty$, giving $d_\infty^2 = \alpha^2 + \beta^2 = \rho_\perp^2 + \rho_\parallel^2 = \rho_1^2 + \rho_2^2$.

3.3 Effective potentials

The qualitative features of the test particle motion in the Kerr metric are usually studied by means of effective potentials, i.e. the functions of r and θ obtained by solving $R(r) = 0$ and $\Theta(\theta) = 0$ (cf. equations 5 and 6) for the constant of motion (for E, say). The first analysis of the latitudinal motion was given by de Felice & Calvani (1972), and was completed by Bičák & Stuchlík (1976b). Since the results are summarized in the literature, we shall not recapitulate them here. We should, however, emphasize that the effective potentials, just as do the right-hand sides of equations (5) and (6) themselves, only in principle determine an accessible region of r- and θ-motion. In the case of (spatially) bound orbits, both radial and latitudinal motion may indeed halt only at those r and θ for which $R(r)$ and $\Theta(\theta)$ vanish or, equivalently, where the particle strikes the curve of its corresponding effective potential. However, an unbound trajectory can end up at *any* θ_∞ permitted by the condition $\Theta(\theta) \geq 0$, since $\dot{\theta}, \ddot{\theta}, \ldots$ vanish asymptotically with $r \to \infty$ as a result of the factor $\Sigma \to \infty$, which enters the left-hand side of (6), rather than because of the vanishing of Θ itself. The root of $\Theta(\theta)$, i.e. the turning 'point' θ_t, may become the asymptotic value of latitude only if, in addition, $\ddot{\theta}_t = 0$. It can be inferred from (9) that this is the case for $\theta_t = \pi/2$ or θ_t satisfying $\sin^2 \theta_t = |\Phi|/(a\sqrt{E^2 - m^2})$.

That the forms of the effective potential cannot determine asymptotic values of θ of unbound trajectories can be seen at first sight on trajectories not having the turning points at all (θs that annul Θ do not exist), although θ_∞s along which particles arrive at radial infinity *do* exist. The same can also be easily understood in the simple example of flat Minkowski space-time in which oblate spheroidal BL coordinates are used. With $M = 0$, $a \neq 0$, the forms of Θ are *the same* as in the curved (Kerr) case. However, plotting a trajectory in Cartesian Kerr–Schild (KS) coordinates (see the next subsection), we immediately deduce the value of θ_∞ that the trajectory will acquire, since it is just a straight line (and θ_∞ is the same in both BL and KS coordinates); but we cannot derive θ_∞ from the effective potentials. This is best seen for $\Phi = 0$ when, by choosing various initial conditions, we arrive at various values of θ_∞, while $\Theta(\theta)$ or the effective potential would at first sight imply $\theta_\infty = 0$ for all trajectories with decreasing θ, since there is no turning point up to $\theta = 0$ (see Appendix B for a more detailed discussion).

As mentioned before, the effective potential generally gives us information on what θ-motion is permitted in principle. In fact, in our discussion in Section 3.1 of particles ejected radially with respect to LNRFs and CFs, we used essentially effective potentials when we determined accessible regions of θ for these particles. As another example, consider the particles ejected from the point given by r_{in} and $\theta_{in} = 0$, i.e. from the axis of symmetry, with initial velocity $\hat{v}_{in}$ and angle $\hat{\alpha}_{in}$, as measured in an LNRF on the axis. A short calculation using $\Theta(\theta) = 0$ and given initial conditions then implies that the value of θ of the particles may increase until the turning point, θ_t, given by the relation

$$\sin^2 \theta_t = \frac{[(r_{in}^2 + a^2)\hat{v}_{in} \sin \hat{\alpha}_{in}]^2}{a^2[(r_{in}^2 + a^2)\hat{v}_{in}^2 - 2Mr_{in}]}. \tag{28}$$

For example, as $r_{in} \to 0$, $\theta_t \to \hat{\alpha}_{in}$. As the last example, notice the simple case of particles launched from the equatorial

plane with $\Phi=0$ ($\beta_{\rm in}=\pi$) when the latitudinal motion is not limited, however small (but non-zero) $\hat{a}_{\rm in}$ might be.

We see that, as much as effective potentials can tell us about some qualitative features of the latitudinal motion, and the above discussion has revealed to us something about possible collimation effects in the Kerr geometry, it is only the direct (numerical) integration of the geodesic equations which yields the real trajectory and, in particular, implies the asymptotic value of θ_∞.

Before presenting the numerical results we first introduce Kerr–Schild coordinates, which will be important in describing trajectories close to the Kerr disc.

3.4 Trajectories in Kerr–Schild coordinates and the Kerr disc

We shall use two coordinate systems to plot the trajectories – Boyer–Lindquist (BL) and Kerr–Schild (KS) coordinates. As was pointed out in Section 2 and at the beginning of Section 3, BL coordinates can be geometrically introduced; only in these coordinates do the geodesic equations separate; and BL coordinates go over into the Schwarzschild coordinates if $a\to 0$. Their astrophysical relevance is apparent: for example, free particles with $\Phi=0$ at rest at infinity fall down to the centre along constant BL latitudes θ. Indeed, BL coordinates are commonly used in discussing processes around Kerr black holes (e.g. Thorne, Price & Macdonald 1986). However, the inner parts of the Kerr space–time are better described in KS coordinates, in which the real nature of the central 'point' $r=0$ emerges. Moreover, KS coordinates become standard Cartesian (Lorentzian) coordinates when $M\to 0$, whereas BL coordinates remain oblate spheroidal – rather than becoming spherical – coordinates in flat space–time.

BL coordinates (t, r, θ, φ) and KS coordinates $(\mathscr{T}, x, y, z)$ are related by (see e.g. Chandrasekhar 1983)

$$\mathrm{d}\mathscr{T}=\mathrm{d}t-\frac{2Mr}{\Delta}\mathrm{d}r, \qquad \mathrm{d}\psi=\mathrm{d}\varphi-\frac{2Ma r}{(r^2+a^2)\Delta}\mathrm{d}r, \tag{29}$$

$$x=\sqrt{r^2+a^2}\,\sin\theta\cos\psi, \qquad y=\sqrt{r^2+a^2}\,\sin\theta\sin\psi, \qquad z=r\cos\theta. \tag{30}$$

Notice that, if $M\to 0$, equations (30) do not change, and equations (29) become $\mathrm{d}\mathscr{T}=\mathrm{d}t$, $\mathrm{d}\psi=\mathrm{d}\varphi$. One may also introduce a flat-space-type cylindrical coordinate $\rho_{\rm f}$ and spherical coordinates $r_{\rm f}$, $\theta_{\rm f}$, by

$$\rho_{\rm f}=\sqrt{x^2+y^2}=r_{\rm f}\sin\theta_{\rm f}=\sqrt{r^2+a^2}\,\sin\theta, \tag{31}$$

$$r_{\rm f}=\sqrt{x^2+y^2+z^2}=\sqrt{\rho_{\rm f}^2+z^2}=\sqrt{r^2+a^2\sin^2\theta}, \tag{32}$$

$$\cos\theta_{\rm f}=z/\sqrt{x^2+y^2+z^2}=z/r_{\rm f}=\cos\theta\,[1+(a^2/r^2)\sin^2\theta]^{-1/2}. \tag{33}$$

Equations (32) and (33) are just the relations between oblate spheroidal and spherical coordinates in flat space. Passing from BL to KS coordinates, the spheres $r=$ constant turn into confocal rotational ellipsoids:

$$\frac{x^2+y^2}{r^2+a^2}+\frac{z^2}{r^2}=1. \tag{34}$$

The point $r=0$ is mapped into a disc given by $x^2+y^2=a^2\sin^2\theta\le a^2$, $z=0$. The cones $\theta=$ constant turn into confocal rotational hyperboloids:

$$\frac{x^2+y^2}{a^2\sin^2\theta}-\frac{z^2}{a^2\cos^2\theta}=1. \tag{35}$$

In particular, the axis ($\theta=0,\pi$) is mapped into $x=y=0$ and the equatorial plane ($\theta=\pi/2$) into $z=0$, $x^2+y^2=r^2+a^2\ge a^2$. The real curvature singularity, $r=0$ and $\theta=\pi/2$, is given by $x^2+y^2=a^2$, $z=0$: it forms the rim of the equatorial disc $r=0$ (cf. Chandrasekhar 1983).

Carter (1966) noticed that the gravitational force exerted on a particle falling down the axis becomes repulsive when $|r|<a$. Israel (1970) constructed the source of the causally maximal extension of the vacuum Kerr metric in the form of a layer of mass with a negative surface density spread over the disc $r=0$, with its singular rim having positively infinite mass so that the total mass of the Kerr space–time is positive. More recently, repulsive effects in the Kerr field were considered by de Felice & Bradley (1988, see also references quoted therein). We shall observe these effects most clearly in the next section.

Obviously, the form of the same trajectory may appear very different when depicted in BL coordinates from its form in KS coordinates, particularly in the innermost regions of the Kerr field (near the disc) where both coordinate systems differ considerably. For example, the trajectories following the lines $\theta=$ constant in the $(\rho=r\sin\theta,\ z=r\cos\theta)$-plane appear deflected towards the equatorial region in the $(\rho_{\rm f}=r_{\rm f}\sin\theta_{\rm f},\ z)$-plane; and those with $\theta_{\rm f}=$ constant in the $(\rho_{\rm f},\ z)$-plane will appear collimated towards the axis in the $(\rho,\ z)$-plane. On the other hand, an 'opposite' effect may also arise: for example, orbits starting from the axis of symmetry under some angle $\hat{\alpha}_{\rm in}<\pi/2$, which are straight lines in the $(\rho_{\rm f},\ z)$-plane, will appear deflected towards the equatorial region in the $(\rho,\ z)$-plane. We should also bear in mind that straight trajectories in the 3-space may appear curved in the meridional projection, and vice versa. The outgoing PNC photons move along outgoing spiralling curves in the 3-space of BL coordinates, though their trajectories project on to straight lines given by $\theta=$ constant in the $(\rho,\ z)$-plane. However, they move along straight lines in KS coordinates (in fact, along the straight generators of hyperboloids $\theta=$ constant), although their trajectories project on to the hyperbolae ($\theta=$ constant) in the $(\rho_{\rm f},\ z)$-plane.

4 NUMERICAL RESULTS

In this section, we present some typical pictures of trajectories obtained by the numerical integration of equations (5) and (6). All of the figures represent trajectories, projected on to the meridional plane, either in BL coordinates, i.e. in the $(\rho,\ z)$-plane, or in KS coordinates, i.e. in the $(\rho_{\rm f},\ z)$-plane. In these figures, we use dimensionless quantities $\rho=(r/M)\sin\theta$, $\rho_{\rm f}=(r_{\rm f}/M)\sin\theta_{\rm f}$ and $z=(r/M)\cos\theta=(r_{\rm f}/M)\cos\theta_{\rm f}$ (cf. Section 3.4). The BL-coordinate mesh, the lines of $r=$ constant and $\theta=$ constant, is illustrated by dotted lines in all of the pictures, the latitudes $\theta=0,\ 15°,\ldots,90°$ being indicated explicitly. We should remember that in general the figures describe different space–times; however, the fact that all radially ejected particles in the Schwarzschild geometry,

and particles ejected radially with parabolic energy in the Kerr geometry, move along θ = constant results in the same 'reference lines' in all figures. In Fig. 2 the stationary limit surfaces $[r = M \pm (M^2 - a^2 \cos^2 \theta)^{1/2}]$ and the event horizons $[r = M \pm (M^2 - a^2)^{1/2}]$ are indicated. In all figures with naked Kerr singularities, the lines $r = a|\cos \theta|$, inside which the repulsive features of the field prevail (see e.g. de Felice & Bradley 1988), are shown by dashed lines (these are just circles given by $\rho_f^2 + z^2 = a^2$ in KS coordinates, and are two circles in BL coordinates). In KS coordinates the Kerr discs are indicated, and the stationary limit surfaces are also shown by solid lines (which always go through the ring singularities. In Figs 2–4, 7 and 8, several trajectories of 'tachyons' (projections of the space-like geodesics) are also plotted in order to get more insight into the character of the Kerr geometry. These are also illustrated by dashed lines.

Since all of the details are given in the figure captions, we confine ourselves to some more general comments here. In the case of a rotating black hole, particles ejected radially with respect to the LNRFs (i.e. along θ = constant and with angular momentum $\Phi = 0$) and with hyperbolic energies escape – in comparison with particles of lower energies – closer to the rotation axis, but the effect is not very large (Fig. 2). It is interesting to note how the orbits of the tachyons (projections of space-like geodesics) smoothly join the high-energy orbits of the real particles, and are collimated towards the rotation axis much more significantly. The picture looks similar in KS coordinates.

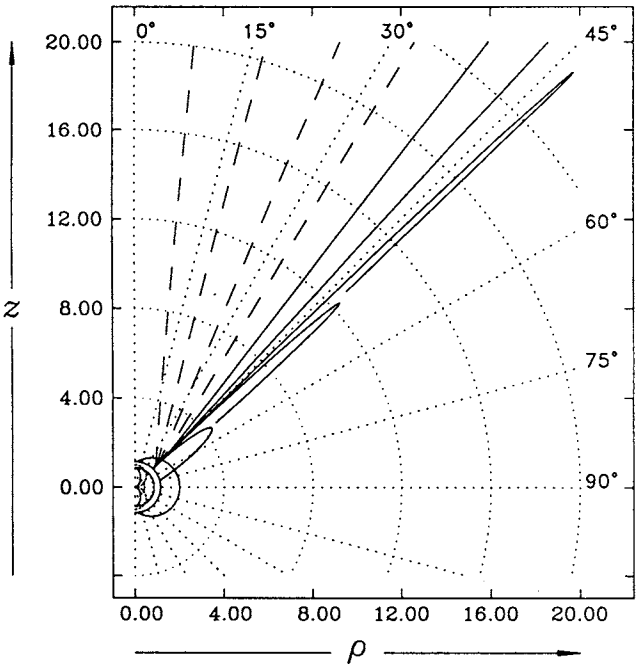

Figure 2. Trajectories of particles ejected radially ($\hat{a}_{in} = 0$) from the LNRF at $r_{in} = 1.15M$, $\theta_{in} = 45°$, from a Kerr black hole with $a = 0.99M$, plotted in BL coordinates. Local initial velocities (from bottom to top in the figure): $\hat{v}_{in} = 0.9992$, 0.999 47, 0.999 52, 0.999 65, 1.0, 1.001, 1.0035. 1.01, 1.03. Corresponding specific energies at infinity: $E/m = 0.745\,577$, 0.915 946, 0.962 458, 1.127 079, ∞; $E/\mathrm{Im}(m) = 0.666\,564$, 0.356 071, 0.210 314, 0.120 825. The orbits of tachyons are indicated by dashed curves.

In the case of naked Kerr singularities, the effect is more pronounced (Fig. 3a). This is primarily due to the fact that particles may be strongly influenced by the Kerr field in the regions close to the disc, and may then move towards more distant regions. However, if the same trajectories are drawn in KS coordinates (Fig. 3b), we observe that, although the orbits corresponding to different energies differ considerably, even the particle with the highest energy does not move along the orbit that would appear to be 'collimated' towards the axis. A first intuitive interpretation suggests that less energetic particles are bent more towards the equatorial plane by the Kerr ring singularity, while the most energetic particles escape little affected. This interpretation works well for radially emitted particles with zero angular momentum. However, we should bear in mind that such a 'Newtonian' picture is not always applicable. For example, as we have already pointed out in Section 3, the PNC photons start in the disc inside the ring singularity, and move outwards to infinity along straight lines in the 3-space of KS coordinates – they are not bent by the ring singularity at all. These photons have angular momenta equal to $aE \sin^2 \theta$, and each of the photons moves along θ = constant (in BL coordinates). Hence in our (two-dimensional) figures they are moving along straight lines, θ = constant, going through the origin in the (ρ, z)-plane, while in the (ρ_f, z)-plane their trajectories project on to hyperbolae given by θ = constant. The orbit of the PNC photons moving along the hyperbola $\theta = 45°$ in the (ρ_f, z)-plane is shown in Fig. 4, where trajectories of other particles ejected radially with respect to the Carter frame are also given. All of these particles have a non-vanishing angular momentum, which makes them less collimated towards the axis than are particles with $\Phi = 0$. Again, tachyons get closer to the axis than do real particles, as was anticipated in Section 3.1. The fact that the effect of some non-zero angular momentum on the motion, and on collimation in particular, is not too large is exhibited in Fig. 5: here we consider two 'cones' of particles – one ejected with hyperbolic velocities, the other with elliptic velocities – which are symmetrical around the radial direction in the LNRFs.

If we were to plot the trajectories of free particles in BL coordinates in flat space–time, we would also find a 'collimation' towards the z-axis; however, for a given initial position and velocity direction, only one orbit would exist along which all particles with different energies move. (A similar picture would arise if we were to plot radial trajectories in the Schwarzschild space–time in spheroidal coordinates.)

In Figs 6(a) and (b) we can see how differently the same trajectories may appear in the BL and KS coordinate systems. Although a collimated jet-like structure in Fig. 6(a) may, in view of Fig. 6(b), appear to be caused just by choosing 'appropriate' initial conditions, we should emphasize again that in both coordinates analogous outgoing particles with parabolic energies would move along θ = constant and hence would fill in the whole quadrant 'uniformly'.

We may therefore say that, in general, particles with hyperbolic energies get closer to the axis of rotation ('are collimated') in comparison with the PNC photons (which represent a natural generalization of outgoing radial photons in the Schwarzschild geometry) and, in particular, in comparison with particles with parabolic energies. Imagine,

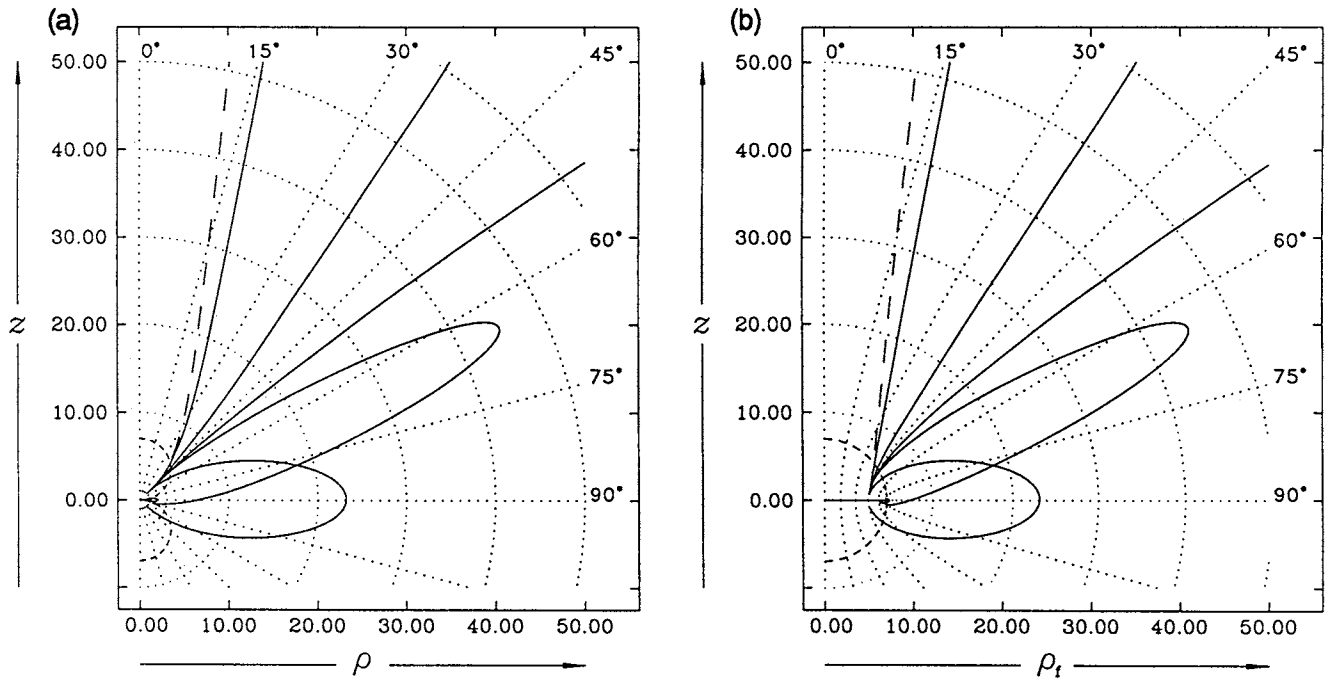

Figure 3. (a) Trajectories of particles ejected radially ($\hat{\alpha}_{in}=0$) from the LNRF at $r_{in}=1.1M$, $\theta_{in}=45°$, from a Kerr naked singularity with $a=7M$, plotted in BL coordinates. Local initial velocities (from bottom to top in the figure): $\hat{v}_{in}=0.0$, 0.2, 0.247, 0.37, 1.0, 4.0. Corresponding specific energies at infinity: $E/m=0.958\,05$, 0.977 806, 0.988 684, 1.031 235, ∞; $E/\mathrm{Im}(m)=0.247\,367$. (b) The same trajectories as in (a) but plotted in KS coordinates [with the BL (r, θ)-grid also indicated].

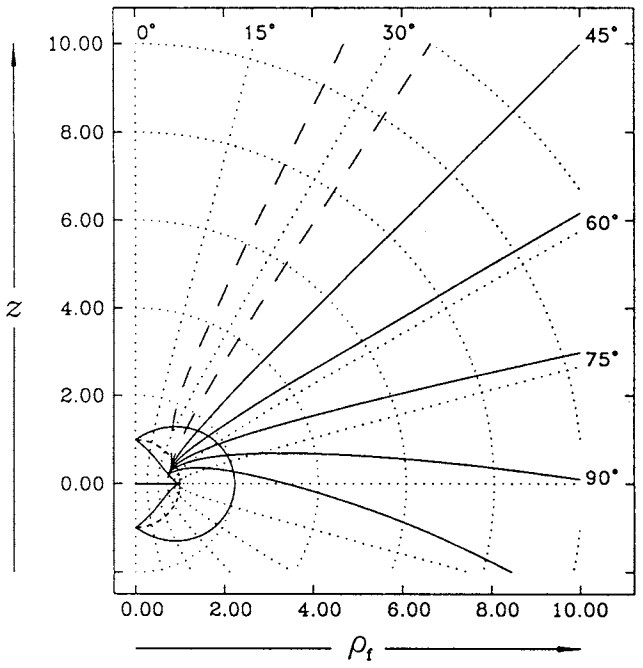

Figure 4. Trajectories of particles ejected radially ($\hat{\alpha}_{in}=0$) from the CF at $r_{in}=0.3M$, $\theta_{in}=45°$, from a Kerr naked singularity with $a=1.000\,001M$, plotted in KS coordinates. Local initial velocities (from bottom to top in the figure): $\hat{v}_{in}=0.0$, 0.3, 0.55, 0.78, 1.0, 1.25, 1.65. Corresponding specific energies at infinity: E/m $=0.911\,323$, 0.955 327, 1.091 19, 1.456 301, ∞; E/Im(m) $=1.215\,098$, 0.694 373.

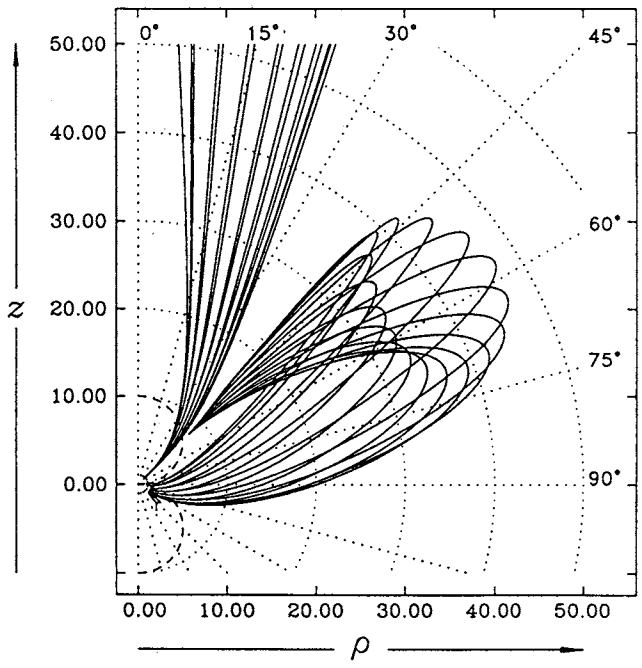

Figure 5. Trajectories of two cones of particles ejected non-radially ($\hat{\alpha}_{in}=10°$, $\hat{\beta}_{in}=0$, 22°5,...,337°5) from the LNRFs at $r_{in}=0.8M$, $\theta_{in}=45°$ (with $\hat{v}_{in}=0.8$, giving $E>m$: typically $E\doteq 1.641m$), and at $r_{in}=8M$, $\theta_{in}=45°$ (with $\hat{v}_{in}=0.3$, giving $E<m$: typically $E\doteq 0.975m$), respectively, from a Kerr naked singularity with $a=10M$, plotted in BL coordinates.

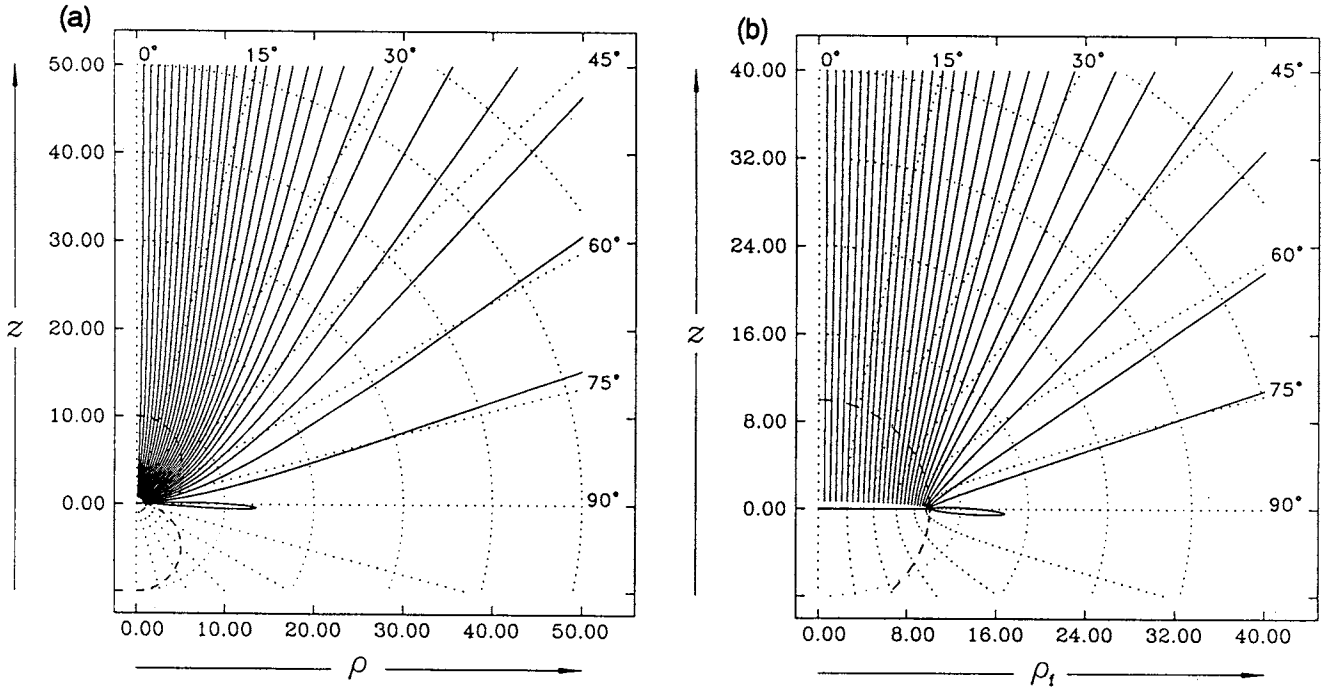

Figure 6. (a) Trajectories of particles ejected radially ($\hat{\alpha}_{in} = 0$) from the LNRFs at $r_{in} = 0.7M$, $\theta_{in} = 87°, 84°, \ldots, 6°, 3°$, with the same local initial velocity $\hat{v}_{in} = 0.77$, from a Kerr naked singularity with $a = 10M$, plotted in BL coordinates. Corresponding specific energies at infinity: $E/m = 0.926\,988, 1.137\,898, \ldots, 1.556\,215, 1.556\,305$. Except for the first (bottom) particle, which has elliptic energy and falls back towards the centre, all other particles have hyperbolic energies and are bent towards the rotation axis, as compared with particles having parabolic energies. (b) The same trajectories as in (a), but plotted in KS coordinates [with the BL (r, θ)-grid also indicated].

for example, that particles fall from rest at infinity with approximately zero angular momentum; assume that at infinity they were distributed isotropically. Now let a mechanism exist in the central regions of the Kerr field, which reflects the particles back into the same directions as measured locally, but also adds some energy to the particles. In the Schwarzschild geometry, the particles would appear at infinity distributed isotropically once more, except that their energies would be higher. In the Kerr geometry, the particles would be collimated towards the rotation axis.

In Fig. 6(b), the repulsive character of the gravitational field in the region close to the axis above the disc is already appearing, since all particles are ejected with the same initial velocity but those ejected from positions closer to the axis arrive at infinity with higher energies than do those starting closer to the ring singularity.

The repulsive character of the Kerr field above the disc is clearly demonstrated in Figs 7–15. The trajectories constructed in these figures also show that the gravitational field in this region can collimate particles considerably. Figs 7(a) and (b) indicate how particles with lower energies become collimated along the axis more than do high-energy particles. As seen in Fig. 7(b), such collimated particles with elliptic energies may escape to distances of $\sim 500M$, where perhaps a non-gravitational force (a radiation drag, say, coming from an accretion disc in the equatorial plane) may accelerate them further along the axis towards infinity. Fig. 8 illustrates how particles ejected towards the disc from the region above the equatorial plane outside the disc and the ring may be repelled above the disc and then start to move upwards closer to the axis. The repulsive effects of the disc and then the attractive effects of the singular ring are clearly seen in Fig. 9, in which trajectories of particles falling from rest towards the disc are presented, as well as in Fig. 10, in which particles with parabolic energies are launched from the axis towards the disc. Fig. 11, in which particles with parabolic energies start from the axis in the directions along the disc, demonstrates how the trajectories are more and more bent towards the axis as their starting points are chosen to be closer and closer to the centre of the disc. Clearly, here the collimation may be described in a completely coordinate-independent way: particles ejected with parabolic energies from the axis in all directions along the disc span locally a solid angle of 2π steradians, but they are collimated into an angle at infinity which is smaller (being zero in the limit) the closer the starting point lies to the centre of the disc. A very suggestive picture of the collimation is seen in Figs 12(a) and (b). Particles with parabolic energies and zero angular momentum ejected from a point situated above the disc (but not on the axis) into the directions spanning 180° locally are collimated into an angle of about 60° at infinity. Fig. 13 shows that such a collimating effect will not be as pronounced for more energetic particles, in particular for photons. However, a non-zero angular momentum will not significantly diminish the collimation of particles with approximately parabolic energies. In Fig. 14, trajectories of particles ejected with the same velocity (as measured in the LNRF) into a solid angle of 2π from the point above the disc support such a conclusion. Finally, in Fig. 15 we see the trajectories of particles with approximately parabolic energies ejected with the same velocity into the 'plane' containing the rotation axis, as measured in the frame tied to the

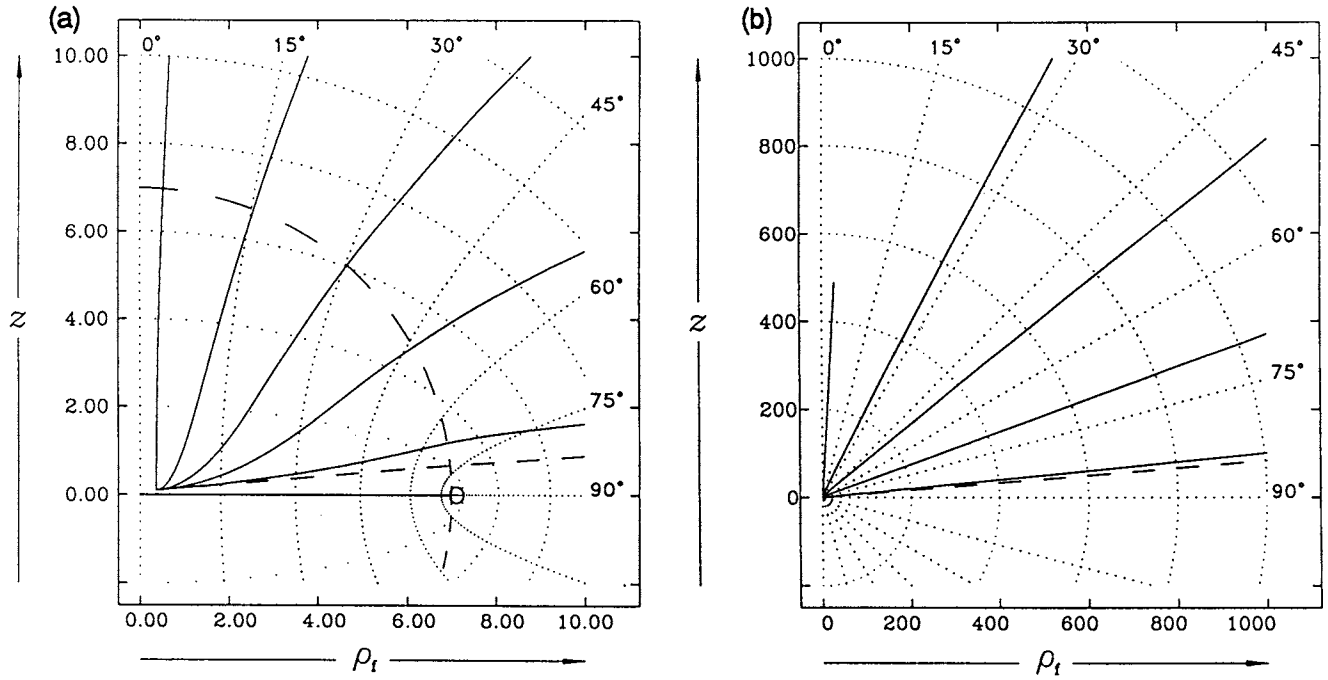

Figure 7. (a) Trajectories of particles launched from the LNRF at $r_{in} = 0.1M$, $\theta_{in} = 3°$, almost along the Kerr disc ($\hat{\alpha}_{in} = 85°$, $\hat{\beta}_{in} = 0$) with $a = 7M$. Local initial velocities (from top to bottom): $\hat{v}_{in} = 0.0$, 0.064, 0.16, 0.32, 1.0, 5.0. Corresponding specific energies at infinity: $E/m = 0.997\,952$, 1.000 002, 1.010 976, 1.053 339, ∞; $E/\mathrm{Im}(m) = 0.203\,706$. Particles with lower energies are collimated significantly along the axis, and receive outwards acceleration as a result of the repulsive field above the disc. (b) The same trajectories as in (a), followed up to $r \sim 1000M$.

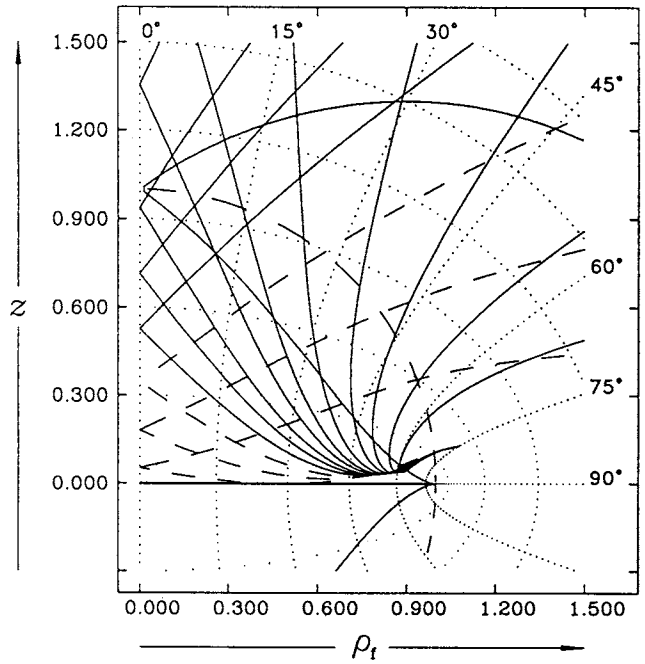

Figure 8. Trajectories of particles launched from the LNRF at $r_{in} = 0.5M$, $\theta_{in} = 75°$, at the local angles $\hat{\alpha}_{in} = 170°$, $\hat{\beta}_{in} = 180°$, towards the Kerr disc with $a = 1.000\,01M$. Local initial velocities (from right to left): $\hat{v}_{in} = 0.945$, 0.9535, 0.9613, 0.9677, 0.974, 0.9794, 0.984, 0.989, 0.994, 1.0, 1.01, 1.025, 1.047 316. Corresponding specific energies at infinity: $E/m = 0.746\,553$, 0.810 156, 0.886 287, 0.968 548, 1.077 809, 1.209 21, 1.370 475, 1.650 777, 2.232 358, ∞; $E/\mathrm{Im}(m) = 1.722\,281$, 1.085 224, 0.784 523. The Kerr ring singularity attracts the particles, but the field above the disc repels them along the axis.

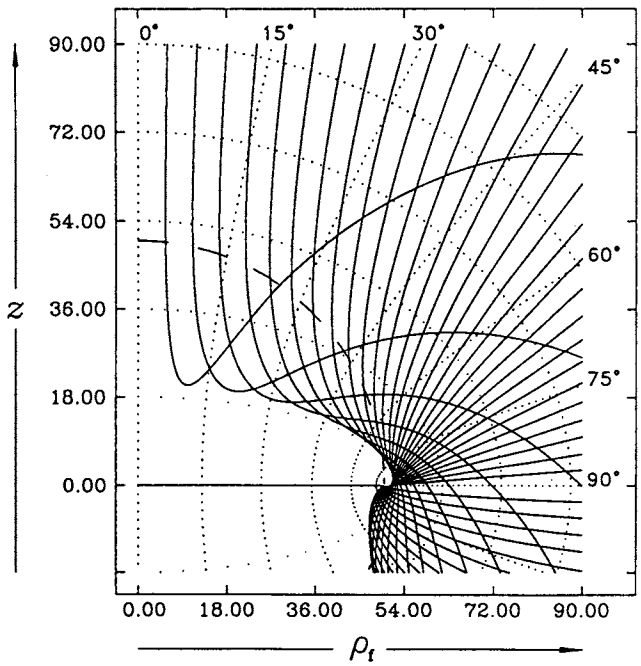

Figure 9. Trajectories of particles falling from rest ($\hat{v}_{in} = 0$) from the LNRFs at $r_{in} = 120M$, $\theta_{in} = 87°, 84°, \ldots, 3°$, towards a Kerr naked singularity with $a = 50M$. All particles are elliptical, with specific energies at infinity ranging from ~ 0.992 to ~ 0.993. The repulsive effect of the disc and the attractive effect of its singular rim are clearly visible.

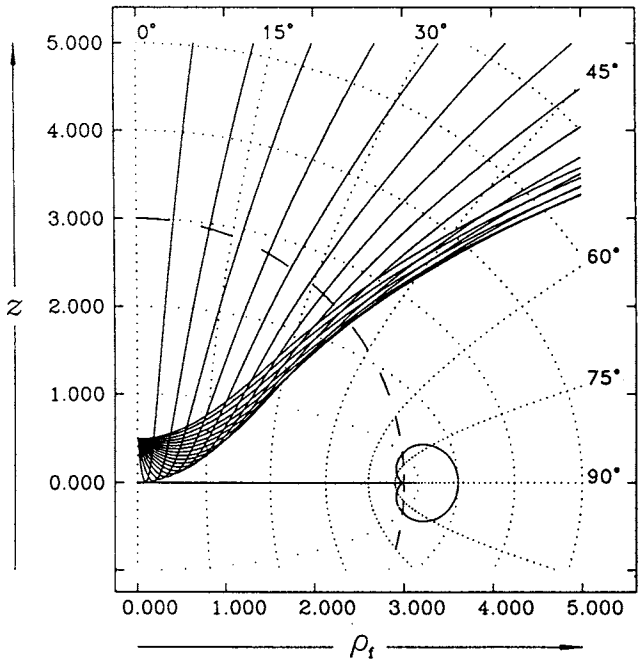

Figure 10. Trajectories of the fan of parabolic particles, launched in various directions ($\hat{\alpha}_{in} = 90°$, 95°, 100°,…, 170°, 175°) from the local frame at $r_{in} = 0.5M$ on the axis ($\theta_{in} = 0$), towards the disc with $a = 3M$. The local initial velocity is $\hat{v}_{in} = 0.328\,798$.

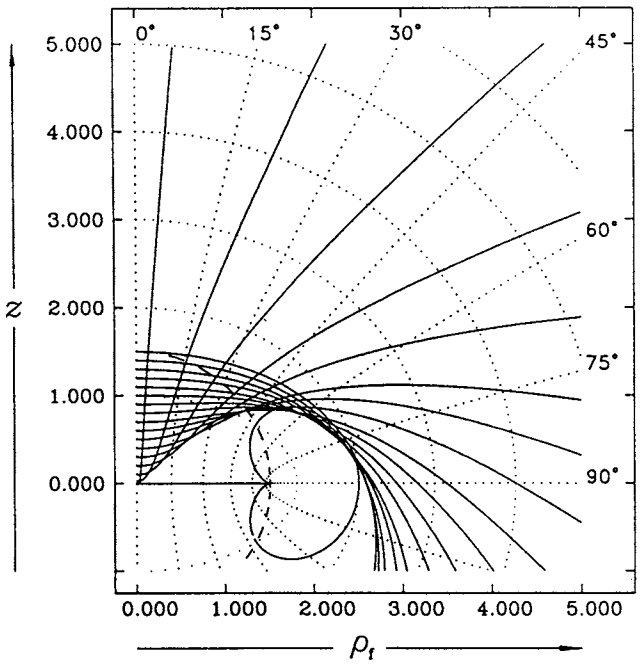

Figure 11. Trajectories of the set of parabolic particles, launched along the central disc ($\hat{\alpha}_{in} = 90°$) with $a = 1.5M$ from the local frames on the axis ($\theta_{in} = 0$). Starting radii: $r_{in}/M = 1.5, 1.4, \ldots, 0.2, 0.1, 0.03, 0.001$. Corresponding local initial velocities: $\hat{v}_{in} = 0.816\,497$, 0.815 526, 0.812 341, 0.806 478, 0.797 395, 0.784 465, 0.766 965, 0.744 065, 0.714 807, 0.678 064, 0.632 456, 0.576 151, 0.506 370, 0.417 938, 0.297 482, 0.163 267, 0.029 815.

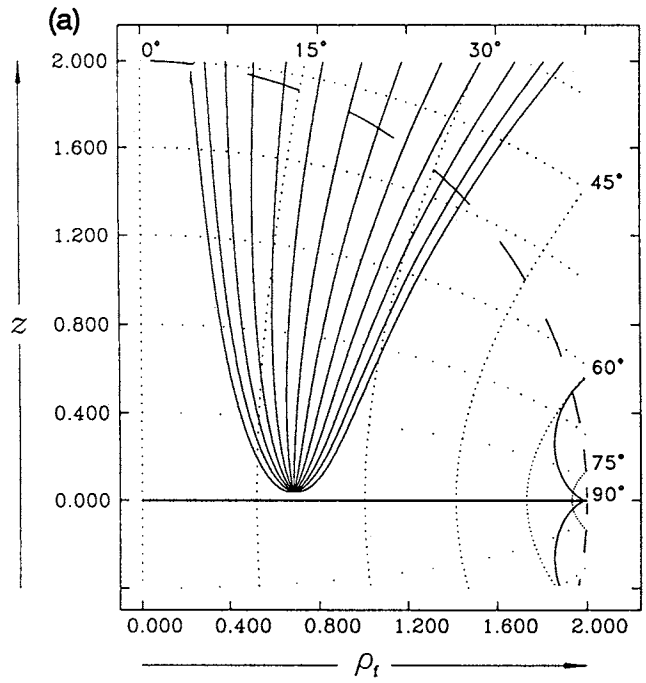

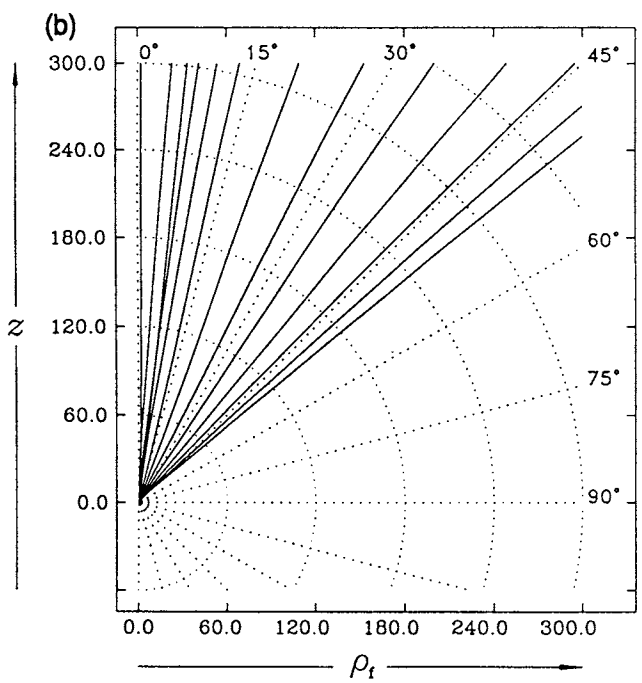

Figure 12. (a) Trajectories of the fan of particles with parabolic energies, ejected above the Kerr disc ($a = 2M$), with the local initial velocity $\hat{v}_{in} = 0.150\,264$ from the LNRF at $r_{in} = 0.04M$, $\theta_{in} = 20°$ in all directions spanning 180° locally: (going from right to left) $\hat{\alpha}_{in} = 90°$, 75°,…, 15°, 0 (with $\hat{\beta}_{in} = 0$), 15°, 30°,…, 75°, 90° (with $\hat{\beta}_{in} = 180°$). (b) The same trajectories as in (a) followed up to $r \sim 300M$. Identification with the trajectories in (a): (from the axis to the equatorial plane) trajectory numbers 10, 11, 9, 12, 13, 8, 7, 6,…, 1; the number is taken from right to left in (a). See also the text for details of this perhaps most illustrative example of collimation.

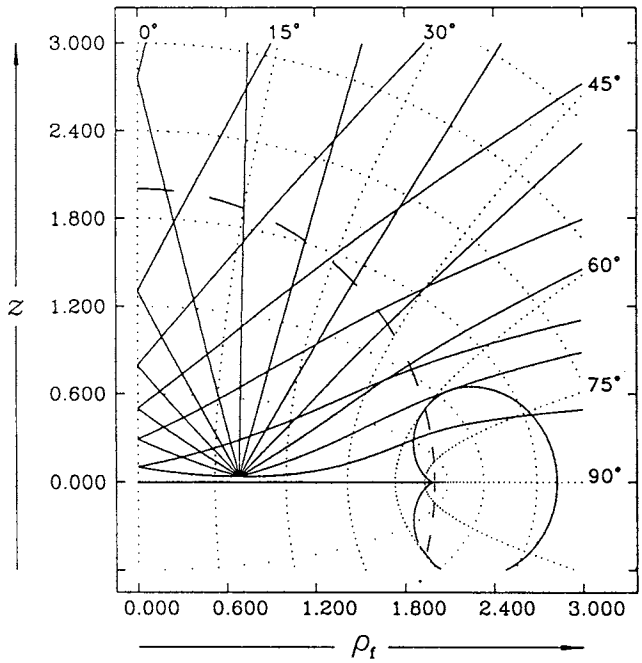

Figure 13. Similar trajectories to those in Fig. 12(a), but with photons ($\hat{v}_{in}=1$).

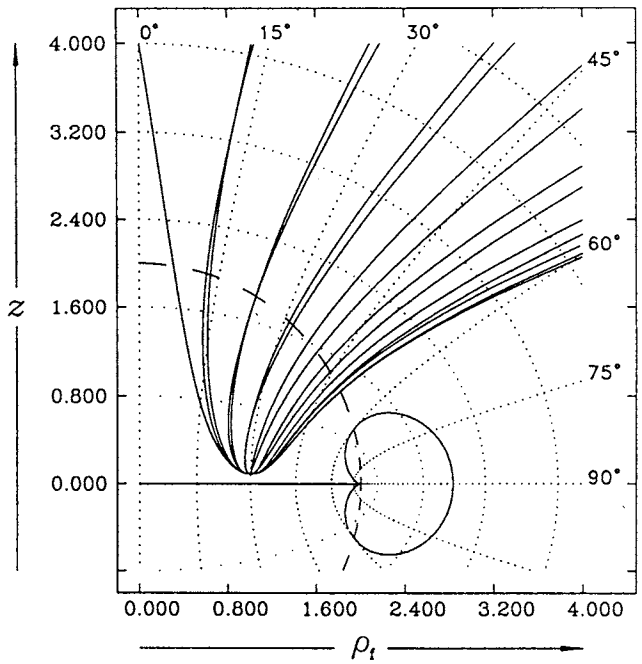

Figure 14. Trajectories of approximately parabolic particles, ejected above the Kerr disc ($a=2M$), with the local initial velocity $\hat{v}_{in}=0.255\,66$ from the LNRF at $r_{in}=0.1M$, $\theta_{in}=30°$ in all directions along the disc $r=0$ ($\hat{\alpha}_{in}=90°$): $\hat{\beta}_{in}=0$, 22°.5,...,90°,..., 180°,...,270°,...,337°.5. Corresponding specific energies at infinity: $E/m=1.0$, 1.003 33, ..., 1.008 703, ..., 1.0, ..., 0.991 297, ..., 0.996 669. 'Approaching', i.e. counter-rotating, particles (corresponding to $180°<\hat{\beta}_{in}<360°$) leave the figure a little to the left of their 'receding', i.e. corotating, counterparts (corresponding to $0<\hat{\beta}_{in}<180°$).

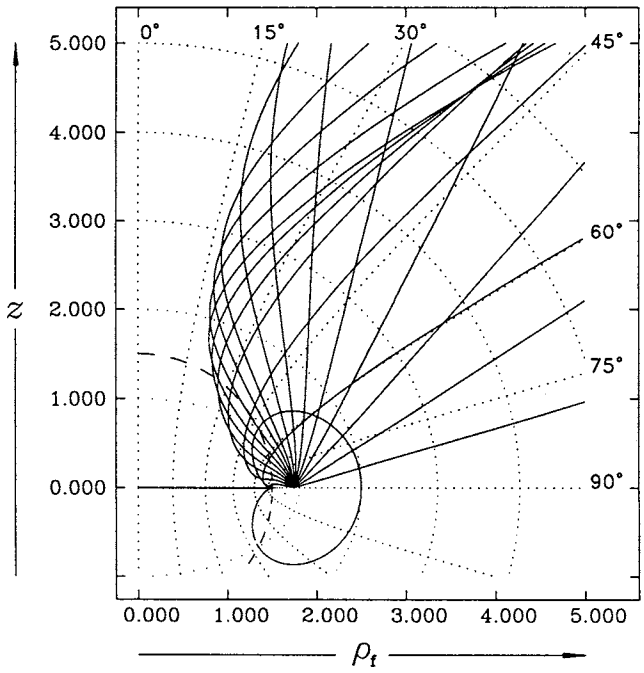

Figure 15. Trajectories of the fan of roughly parabolic particles ($E\doteq 1.001m$), launched at the angles $\hat{\alpha}_{in+}=10°$, 20°,...,170°, $\hat{\beta}_{in+}=180°$ from the local tetrad tied to the particle that freely orbits in the 'prograde' marginally stable orbit (at $r_{in}=0.879\,35M$, $\theta_{in}=90°$) around a Kerr naked singularity with $a=1.5M$. The local initial velocity is $\hat{v}_{in+}=0.871$. Here the influence of the source is combined with the centrifugal influence of Φ ($=0.47mM$), which prevents the particles reaching the axial region.

particle that is freely orbiting along the 'prograde' marginally stable circular orbit in the equatorial plane. All of the particles have the same non-zero angular momentum, the 'centrifugal' effect of which is combined with the repulsive character of the region above the Kerr disc. Nevertheless, the particles ejected towards the axis get repelled and are collimated 'upwards' along the rotation axis.

5 CONCLUDING REMARKS

Our calculations indicate that latitudinal anisotropy of the geometry around a rotating source influences the latitudinal motion of particles ejected from central regions. In general, it leads to the collimation of particles with higher energies towards the rotation axis, as compared with particles with parabolic or lower energies. Although, in this sense, relativistic particles are collimated by a rapidly rotating black hole, the effect appears not to be large enough to be astrophysically very important in the case of the Kerr hole. On the other hand, our calculations show that, even if some cosmic jets originate close to a central, rapidly rotating black hole, the influence of Kerr geometry will not significantly disturb collimation effects resulting from other (non-geometrical) causes. (In this context, let us mention that, in principle, geometrical effects of the magnetic field around a Schwarzschild black hole might imply collimation effects, as indicated recently by Karas & Vokrouhlický 1990).

Furthermore, our results show that there are essential differences between the manifestations of space-times with naked singularities and those of space-times with singularities hidden inside horizons. We have seen that, if the repulsive region around the disc spanning the Kerr ring singularity can manifest itself to a distant observer, it may collimate the particles along the rotation axis very significantly. Here, low-energy particles become more collimated than do those with high energies, as the 'Newtonian intuition' suggests. Moreover, the repulsive effects of a naked Kerr geometry occur close to the rotation axis (rather than in the equatorial plane), so that a mechanism is provided for particle acceleration along this axis. A Kerr naked singularity can also be understood as a prototype of the 'source' of an asymptotically flat stationary geometry with angular momentum, so that it might be expected that the geometries around more general, rotating naked singularities will exhibit similar effects as well. Of course, naked singularities would be expected to have a 'quantum nuclear region', and only outside it might classical solutions describe the space-time geometry.

An unorthodox conclusion would be to suggest, on the basis of the ability of the field of a Kerr naked singularity to collimate (and accelerate) particles close to the disc spanning the singularity, that this type of object could account for the initial collimation of cosmic jets. Despite the work of Nakamura et al. (1987), indicating that not all collapses with rotation lead to the formation of a Kerr black hole, and despite the very recent work of Shapiro & Teukolsky (1992, and references therein) indicating that naked singularities may form in general relativity, such a suggestion is, needless to say, speculative. The cosmic censorship conjecture remains a plausible – though difficult to prove – hypothesis. In their recent paper, 'On the outcome of Kerr-like collapse', Charlton & Clarke (1990) draw an appropriate conclusion: 'the development of numerical work...should soon provide a complete answer to the question of whether there is a physically significant range of cases in which gravitational collapse leads to a ring singularity, as opposed to a black hole'.

ACKNOWLEDGMENTS

JB thanks Professor Donald Lynden-Bell for kind hospitality at the Institute of Astronomy in Cambridge, and for several very helpful discussions. The authors are most grateful to Dr Michael Ingham, and by no means only for improving the English in the manuscript. This work has been partly supported by internal grant No. 30305 of the Czechoslovak Academy of Sciences.

REFERENCES

Bardeen J. M., 1973, in DeWitt C., DeWitt B. S., eds, Black Holes. Gordon and Breach, New York, p. 230
Bardeen J. M., Press W. H., Teukolsky S. A., 1972, ApJ, 178, 347
Begelman M. C., Blandford R. D., Rees M. J., 1984, Rev. Mod. Phys., 56, 255
Bičák J., Stuchlík Z., 1976a, MNRAS, 175, 381
Bičák J., Stuchlík Z., 1976b, Bull. Astron. Inst. Czech., 27, 129
Bičák J., Stuchlík Z., Balek V., 1989a, Bull. Astron. Inst. Czech., 40, 65
Bičák J., Stuchlík Z., Balek V., 1989b, Bull. Astron. Inst. Czech., 40, 133
Bičák J., Semerák O., Hadrava P., 1992, in Sato H., Nakamura T., eds, Proc. Sixth Marcel Grossmann Meeting on General Relativity. World Scientific, Singapore, p. 674
Blandford R. D., 1987, in Zensus J. A., Pearson T. J., eds, Superluminal Radio Sources. Cambridge Univ. Press, Cambridge, p. 310
Carter B., 1966, Phys. Rev., 141, 1242
Carter B., 1968, Phys. Rev., 174, 1559
Carter B., 1987, in Carter B., Hartle J. B., eds, Gravitation in Astrophysics (Cargèse 1986). Plenum Press, New York, p. 63
Chandrasekhar S., 1983, The Mathematical Theory of Black Holes. Clarendon Press, Oxford
Charlton N., Clarke C. J. S., 1990, Class. Quantum Grav., 7, 743
Contopoulos G., 1984, Gen. Relativ. Gravitation, 16, 43
de Felice F., 1975, A&A, 45, 65
de Felice F., Bradley M., 1988, Class. Quantum Grav., 5, 1577
de Felice F., Calvani M., 1972, Nuovo Cim., 10B, 447
de Felice F., Calvani M., 1979, Gen. Relativ. Gravitation, 10, 335
de Felice F., Yu Y., 1982, J. Phys. A, 15, 4431
Dymnikova I. G., 1986, Sov. Phys.-Usp., 29, 215
Floyd R. M., Shepee B. A., 1972, Int. J. Theor. Phys., 6, 281
Goldstein H., 1974, Z. Phys., 271, 275
Israel W., 1970, Phys. Rev. D, 2, 641
Johnston M., Ruffini R., 1974, Phys. Rev. D, 10, 2324
Karas V., Vokrouhlický D., 1990, Class. Quantum Grav., 7, 391
Lake K., Zannias T., 1990, Phys. Rev. D, 41, 3866
Lake K., Hood K., Stone J., 1984, Gen. Relativ. Gravitation, 16, 541
Miller J. C., de Felice F., 1985, ApJ, 298, 474
Misner C. W., Thorne K. S., Wheeler J. A., 1973, Gravitation. Freeman, San Francisco
Nakamura T., Oohara K., Kojima Y., 1987, Prog. Theor. Phys. Suppl., 90, 1
Shapiro S. L., Teukolsky S. A., 1992, Phys. Rev. D, 45, 2006
Sharp N. A., 1979, Gen. Relativ. Gravitation, 10, 659
Stewart J., Walker M., 1973, Springer Tracts Mod. Phys., 69, 69
Stoghianidis E., Tsoubelis D., 1987, Gen. Relativ. Gravitation, 19, 1235
Thorne K. S., Price R. H., MacDonald D. A. (eds), 1986, Black Holes: The Membrane Paradigm. Yale Univ. Press, New Haven
Yakovlev D. G., 1975, Zh. Eksp. Teor. Fiz., 68, 369
Znajek R. L., 1977, MNRAS, 179, 457

APPENDIX A: PARAMETRIZATION OF CONSTANTS OF MOTION IN THE LOCAL FRAMES

Constants of motion, E, Φ and K, can be expressed in terms of more intuitive quantities – the components of the 4-momentum of the particle as measured in a frame (tetrad) at a given point at which the particle is instantaneously located. In the Kerr geometry, the frames $\{\boldsymbol{e}_{\hat{\alpha}}\}$ carried by (tied to) observers orbiting uniformly along circles ('φ-lines') at given r, θ are usually chosen, with the observers' 4-velocity $\boldsymbol{u}=\boldsymbol{e}_{\hat{0}}$ and unit spatial vectors $\boldsymbol{e}_{\hat{i}}$ pointing in the directions of global space (e.g. Boyer–Lindquist) coordinates.

In this Appendix, we shall write down the final results for several sets of frames arising naturally in the Kerr field – in the (commonly used) locally non-rotating frame tied to zero-angular-momentum orbiters (e.g. Bardeen et al. 1972), in the Carter frame (e.g. Znajek 1977; Carter 1987), and in the frames connected with the 'static' observers and with observers orbiting freely at $(r,\ \theta)=$constant. More details about these frames and about their interrelation will be given elsewhere (Semerák, in preparation).

The quantities measured in a *general* frame at a given point will be denoted by a hat above and a capital F below the quantity – e.g. $\underset{\mathrm{F}}{v^i}$, $\underset{\mathrm{F}}{\hat{E}}$ stand for the locally measured velocity and energy of the particle. In particular, we shall use just the hats (without F below the quantity) to denote the quantities in the locally non-rotating frame (LNRF); we shall use tildes to denote quantities with respect to the Carter frame (CF), bars to represent quantities with respect to the static frame (SF), and breves to denote quantities with respect to the frame tied to the freely orbiting observer at given r, θ (the FF frame). Given any frame $e^{\mu}_{\hat{a}}$, there exists a dual frame $e^{\hat{a}}_{\mu}$ such that $e^{\mu}_{\hat{a}} e^{\hat{\beta}}_{\mu} = \delta^{\hat{\beta}}_{\hat{a}}$ and $e^{\mu}_{\hat{a}} e^{\hat{a}}_{\nu} = \delta^{\mu}_{\nu}$: the frame indices are shifted by the Minkowski metric $\eta_{\mu\nu}$.

Now, by projecting the 4-momentum of the particle on to a frame $p_{\mu} = e^{\hat{a}}_{\mu} \underset{\mathrm{F}}{p_{\hat{a}}}$, the constants of motion Φ, E and K (see e.g. Misner, Thorne & Wheeler 1973; Chandrasekhar 1983, for their definition) can be rewritten as follows:

$$\Phi = p_{\varphi} = -e^{\hat{t}}_{\varphi} \underset{\mathrm{F}}{p^{\hat{t}}} + e^{\hat{\varphi}}_{\varphi} \underset{\mathrm{F}}{p^{\hat{\varphi}}}, \tag{A1}$$

$$E = -p_t = e^{\hat{t}}_{t} \underset{\mathrm{F}}{p^{\hat{t}}} - e^{\hat{\varphi}}_{t} \underset{\mathrm{F}}{p^{\hat{\varphi}}} = \frac{1}{u^t} \underset{\mathrm{F}}{p^{\hat{t}}} + \omega_{\mathrm{F}} \Phi, \tag{A2}$$

$$K = \frac{P^2}{\Delta} - m^2 r^2 - \Delta p_r^2 = \frac{P^2}{\Delta} - m^2 r^2 - \Sigma (\underset{\mathrm{F}}{p^{\hat{r}}})^2, \tag{A3}$$

or, in terms of the latitudinal component of the particle's momentum,

$$K = T^2 + (ma\cos\theta)^2 + p_{\theta}^2 = T^2 + (ma\cos\theta)^2 + \Sigma (\underset{\mathrm{F}}{p^{\hat{\theta}}})^2. \tag{A4}$$

Here, Δ, Σ, P and T are given in Section 2, and

$$\omega_{\mathrm{F}} = (\mathrm{d}\varphi/\mathrm{d}t)_{\mathrm{F}}, \qquad u^t = (-g_{tt} - 2\omega_{\mathrm{F}} g_{t\varphi} - \omega_{\mathrm{F}}^2 g_{\varphi\varphi})^{-1/2} \tag{A5}$$

denote the (coordinate) angular velocity and the dilation factor of the observers who orbit along the φ-lines and to whom is tied a set of frames, in particular one of those mentioned above. The frame components of the particle's 4-momentum can be written in terms of quantities directly measurable in the given frame. The usual 3-velocity of the particle is

$$\underset{\mathrm{F}}{v^i} = \underset{\mathrm{F}}{\hat{v}}\, \underset{\mathrm{F}}{n^i}, \qquad \underset{\mathrm{F}}{\hat{v}^2} = \eta_{ij} \underset{\mathrm{F}}{v^i} \underset{\mathrm{F}}{v^j}, \tag{A6}$$

where

$$\underset{\mathrm{F}}{n^{\hat{r}}} = \cos \underset{\mathrm{F}}{\hat{\alpha}}, \qquad \underset{\mathrm{F}}{n^{\hat{\theta}}} = \sin \underset{\mathrm{F}}{\hat{\alpha}} \cos \underset{\mathrm{F}}{\hat{\beta}}, \qquad \underset{\mathrm{F}}{n^{\hat{\varphi}}} = \sin \underset{\mathrm{F}}{\hat{\alpha}} \sin \underset{\mathrm{F}}{\hat{\beta}}, \tag{A7}$$

$\underset{\mathrm{F}}{\hat{\alpha}}$, $\underset{\mathrm{F}}{\hat{\beta}}$ denoting local latitudinal and azimuthal angles in the observer's frame (see Fig. 1); and the locally measured energy of the particle is simply

$$\underset{\mathrm{F}}{\hat{E}} = m/\sqrt{1 - \underset{\mathrm{F}}{\hat{v}^2}}. \tag{A8}$$

In terms of these quantities, we have

$$\underset{\mathrm{F}}{p^{\hat{t}}} = \underset{\mathrm{F}}{\hat{E}}, \qquad \underset{\mathrm{F}}{p^i} = \underset{\mathrm{F}}{\hat{E}}\, \underset{\mathrm{F}}{v^i}. \tag{A9}$$

Now, in the case of LNRFs tied to zero-angular-momentum orbiters, we have $\omega_{\mathrm{F}} = \omega$, where ω is just given by equation (3). The relations (A1) and (A2) then take the form

$$\Phi = \sqrt{\frac{\mathscr{A}}{\Sigma}}\, \hat{E} v^{\hat{\varphi}} \sin\theta, \tag{A10}$$

$$E = \sqrt{\frac{\Delta\Sigma}{\mathscr{A}}}\, \hat{E} + \omega\Phi. \tag{A11}$$

In the case of the Carter frame (CF), $\omega_{\mathrm{F}} = a/(r^2 + a^2)$. One then finds that

$$\Phi = \frac{\sin\theta}{\sqrt{\Sigma}} \tilde{E} [a\sqrt{\Delta}\sin\theta + (r^2 + a^2) v^{\tilde{\varphi}}], \tag{A12}$$

$$E = \frac{\tilde{E}}{\sqrt{\Sigma}} (\sqrt{\Delta} + a v^{\tilde{\varphi}} \sin\theta). \tag{A13}$$

For the frames connected with the observers who are static in Boyer–Lindquist coordinates, we have $\omega_{\mathrm{F}} = 0$. This implies that

$$\Phi = \frac{\sin\theta}{\sqrt{\Sigma - 2Mr}} \bar{E} \left(\sqrt{\Delta\Sigma}\, v^{\bar{\varphi}} - \frac{2Mr}{\sqrt{\Sigma}} a \sin\theta \right), \tag{A14}$$

$$E = \sqrt{1 - \frac{2Mr}{\Sigma}}\, \bar{E}. \tag{A15}$$

Finally, let us consider frames tied to observers who are falling freely along φ-lines. Neglecting (unstable) positions at rest on the symmetry axis at $r = \pm a$, only circular orbits in the equatorial plane (either prograde with $\Phi > 0$, or retrograde with $\Phi < 0$) exist. We find that the constants of motion then read as follows:

$$\Phi = \frac{\breve{E}_{\pm}}{\sqrt{Z_{\pm}}} \{\sqrt{M}[\pm (r^2 + a^2) - 2a\sqrt{Mr}] + \sqrt{\Delta}(r^{3/2} \pm a\sqrt{M}) v^{\breve{\varphi}}_{\pm}\}, \tag{A16}$$

$$E = \frac{\breve{E}_{\pm}}{\sqrt{Z_{\pm}}} (r^{3/2} - 2M\sqrt{r} \pm a\sqrt{M} \pm \sqrt{M\Delta}\, v^{\breve{\varphi}}_{\pm}), \tag{A17}$$

where

$$Z_{\pm} = r(r^2 - 3Mr \pm 2a\sqrt{Mr} + 4M^2), \tag{A18}$$

with the plus (minus) sign for prograde (retrograde) orbits.

Note that the constant K is expressed by (A3) and (A4) in all orbiting frames considered, since the frame vectors $\boldsymbol{e}_{\hat{r}} = \sqrt{(\Delta/\Sigma)}(\partial/\partial r)$, $\boldsymbol{e}_{\hat{\theta}} = (1/\sqrt{\Sigma})(\partial/\partial\theta)$ are the same in these frames.

APPENDIX B: CRITICAL REVIEW OF PREVIOUS NUMERICAL RESULTS

As mentioned in the Introduction, only the work of Lake et al. (1984, hereafter LHS) was devoted to the numerical study of the latitudinal and radial motion of the particles in the Kerr geometry, which is relevant to the collimation effects. In that work, however, no such effects were discovered, and the repulsive region around the ring singularity remained unnoticed. In this Appendix, we briefly discuss the conclusions of LHS in the light of our results described in the main text of this paper. We assume that an interested reader has the paper by LHS at his disposal.

First of all, LHS present all of their numerical results in BL coordinates, so that it is not very surprising that the region

around the ring singularity was not treated properly. Nevertheless, regarding our results, we can understand their figs 2, 3 and 6 as the effect of the choice of r_{in}, Φ and K rather than of a and E. LHS plot $\log(r/M)\sin\theta$ and $\log(r/M)\cos\theta$ along 'x, y'-axes. (Note that they erroneously write $\log[(r/M)\sin\theta]$, $\log[(r/M)\cos\theta]$ on p. 544. Note also that the logarithmic projection itself deforms the trajectories and makes their intuitive interpretation harder.) Now, in their figs 2 and 3, the trajectories with given constants of motion are plotted for different values of the Kerr parameter a; all trajectories start 'at the origin' (i.e. at $r_{in}=M$) and at $\theta_{in}\doteq 13°$. As the parameter a increases (for example, in fig. 2, $a=0.1$–1000), the trajectories get 'quickly' bent towards the equatorial plane. This, according to LHS, should demonstrate the effect of the angular momentum of the source on the latitudinal motion. Such a conclusion is, however, not correct. First, by plotting trajectories for different values of a, they compare different space–times in the same figure. Secondly, by increasing a, but keeping $r_{in}=M$, one effectively changes (decreases) r_{in} because in KS coordinates (in which the innermost region is represented properly) the Kerr ring is located at $\rho_f=a$. (For example, in fig. 2 of LHS, r_{in} decreases by a factor of 10^4 with respect to a.) In KS coordinates, it is intuitively seen that, with $\theta_{in}\doteq 13°$, the increase of a (r_{in} being kept fixed) makes the attraction of the ring more effective in bending the trajectories towards the equatorial plane. One might object that this could be compensated by the repulsion of the disc, which gets stronger with decreasing r_{in}. However, there is a third effect, which must be taken into account. When changing a, LHS keep their constant L (given in their equation 3) fixed, and thus increase Φ and K. (For example, in their fig. 2, Φ increases by a factor of 10^4 and K by a factor of 10^8: from $\Phi=0.0102mM$, $K=0.009\,95m^2M^2$ to $\Phi=102mM$, $K=995\,000m^2M^2$.) Such an increase of Φ and K implies that the trajectories turn away from the axis and that their latitude varies more, as one can understand from our analytical considerations (cf. Section 3.1), from numerical simulations and, in fact, from fig. 7 of LHS.

The effect of increasing Φ and K leads to another misunderstanding when LHS compare their fig. 3 ('high-energy trajectories') with their fig. 2 ('low-energy trajectories') and conclude that here the influence of the energy of the test particles on their latitudinal motion is revealed. (A similar interpretation of 'the effect of energy' is made from figs 5, 6 and 9.) The high-energy trajectories contained in these figures appear to be more influenced by the Kerr field than are those corresponding to particles with low energies – against both intuition and our results presented in this paper. The explanation comes again from the fact that LHS, when increasing energy, keep their constant L fixed, and hence increase Φ and K: e.g. Φ increases by a factor of 110 and K by a factor of 1516 when going from their fig. 2 to fig. 3, while the energy increased by a factor of 45.

Furthermore, it is clear that LHS did not even notice the 'collimation effects' that we found in BL coordinates (cf. our Figs 2–6). Specifically, they choose θ_{in} to be equal to (or very close to) θ_{min}, i.e. at the turning points of the latitudinal motion, from which the particle's latitude θ cannot decrease. Since LHS always choose $\theta_{in}\doteq\theta_{min}$, it is not helpful to compare their figs 5 and 9, which differ only in the sign of $\dot\theta_{in}$.

Some additional statements of LHS should be corrected: for example, 'neither the sign of Φ nor the initial value of r/M has an important effect on the evolution of the trajectories in the r–θ subspace' – see the discussion above, and the role of Φ in equations (5) and (6) in the main text of this paper, or consider, for example, two particles ejected from the symmetry axis with the same constants of motion but from very different r_{in}s. Equation (5) of LHS is valid for hyperbolic trajectories only; the equality in (5) holds necessarily at the axis of symmetry also, etc.

We should emphasize that the trajectories constructed numerically by LHS are correct; however, they are not representative of the latitudinal and radial motion in the Kerr field, and their interpretation, as given by LHS, is either false or not clear.